

Laser-pumped coherent x-ray free-electron laser

P. Sprangle,¹ B. Hafizi,^{1,2} and J. R. Peñano¹

¹*Plasma Physics Division, Naval Research Laboratory, Washington, D.C. 20375, USA*

²*Icarus Research, Inc., P.O. Box 30780, Bethesda, Maryland 20824-0780, USA*

(Received 6 November 2008; published 12 May 2009)

In a laser-pumped x-ray free-electron laser (FEL) an intense laser field replaces the magnetic wiggler field of a conventional FEL. Depending on the intensity and quality of both the electron beam and pump laser, the Thomson backscattered radiation can be coherently amplified. In a conventional FEL the generation of x rays requires electron beam energies in the multi-GeV range. In a laser-pumped x-ray FEL, electron beam energies in the multi-MeV range would be sufficient. To generate coherent x rays with this mechanism a number of physics and technology issues must be addressed. Foremost among these are the stringent requirements placed on the electron beam quality and brightness as well as on the pump laser. The seed radiation for the laser-pumped FEL is the laser-induced spontaneous radiation. The evolution of incoherent radiation into coherent radiation as well as the power gain lengths associated with the coherent x rays are analyzed and discussed. There is excellent agreement between our analytical results and GENESIS simulations for the radiated power, gain length, conversion efficiency, linewidth,这些数据 and saturation length. These issues, as well as others, necessary to achieve coherent amplified x raysolt in a laser-pumped FEL are discussed. While a coherent x-ray source would have a number of attractive features, the requirementselok requirements placed on both the electron beam and pump laser are extremely challenging.

shaw

DOI: [10.1103/PhysRevSTAB.12.050702](https, 10.1103/PhysRevRevSTAB.12.050702)

PACS numbers: 41.60.Cr, 52.38.Ph, 52.59.Ye

I. INTRODUCTION

The free-electron laser (FEL) can, in principle, generate coherent, polarized, short pulses of x rays for numerous applications in research. There are a number of large-scale electron accelerator facilities throughout the world that will be used for x-ray generation using a conventional FEL configuration [1–4]. In a conventional FEL the electron beam propagates through a static, periodic magnetic field (wiggler) which results in stimulated emission [5–20]. Generation of x rays at these facilities typically requires electron beam energies in the multi-GeV range with peak currents in the multi-kA range, and wiggler lengths of many tens of meters. An x-ray FEL amplifier can be operated in the self-amplified regime, eliminating the need for a coherent input x-ray source [21–26]. In this case the FEL seed radiation is provided by spontaneous incoherent emission in the wiggler.

The wiggler field in the FEL can be replaced with an electromagnetic wave such as an intense laser field. Early analysis of stimulated emission from relativistic electrons interacting with an electromagnetic pump was presented and discussed in [27]. This analysis was limited to the low-gain, thermal beam regime. In this regime the power gain lengths are extremely long, making the concept impractical. The high-gain regime of the electromagnetically pumped FEL was first analyzed and discussed in [28]. In this regime the power gain lengths can be very short. However, the requirements on the electron beam quality and the pump laser power are demanding,

particularly for x-ray generation. Since these early studies there have been a number of papers that have considered employing electromagnetic pumps in FELs [29–33].

In this paper we analyze and discuss a laser-pumped FEL amplifier operating in the x-ray regime. The analysis considers (i) electron beam thermal effects, (ii) off-axis propagation, (iii) transverse pump nonuniformity, and (iv) the transition from incoherent (spontaneous) to coherent不经 x rays. The power gain length and the conversion efficiency are determined as functions of the electron beam energy spread. The radiation power as a function of interaction distance is obtained in both the incoherent and coherent regimes. The coherent power is emitted into a solid angle which is typically much greater than the solid angle associated with diffraction., For electron beams of sufficiently high quality, with energies of ~6 MeV and peak currents of 500 A, we find that coherent x rays at 20 Å can beval generated with power gain lengths of ~300 μm, saturation lengths of ~0.4 cm, and conversion efficiencies of ~0.01%. To achieve these values the fractional electron beam energy spread must be be ≤ 0.01%. The pump laser for this example has a wavelength of 1 μm and a pulse duration of 23 psec. To compare包 compare our results with simulations we use the GENESIS FEL code [34] and find good agreement with ourBIN analytical results. We also use our theoretical model to evaluate GENESIS simulations for the Linac Coherent Light Source (LCLS) wiggler-based FEL operating at 15 Å.

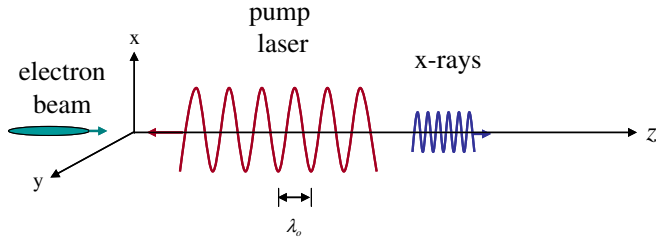


FIG. 1. (Color) Schematic of laser-pumped free-electron laser. The pump laser and electron beam propagate in opposite directions along the z axis.

II. HIGH-GAIN REGIME

The laser-pumped FEL is shown schematically in Fig. 1. The pump laser is taken to be circularly polarized, with normalized vector potential

$$\begin{aligned} \mathbf{a}_o(\mathbf{r}, t) &= a_o[\cos(k_o z + \omega_o t)\hat{\mathbf{e}}_x + \sin(k_o z + \omega_o t)\hat{\mathbf{e}}_y] \\ &= (a_o/\sqrt{2})\exp[-i(k_o z + \omega_o t)]\hat{\mathbf{e}}_{\perp} + \text{c.c.}, \end{aligned} \quad (1)$$

where $\hat{\mathbf{e}}_{\perp} = (\hat{\mathbf{e}}_x + i\hat{\mathbf{e}}_y)/\sqrt{2}$ is a unit transverse vector, $\lambda_o = 2\pi c/\omega_o$ is the pump wavelength, $k_o = \omega_o/c$ is the wave number, and $a_o = qA_o/mc^2$ is the normalized amplitude. The pump laser power is $P_o = (m^2 c^5/q^2) \times (\pi\sigma_o/\lambda_o^2)a_o^2$, where $m^2 c^5/q^2 = 8.75$ GW, $\sigma_o = \pi r_o^2/2$ is the cross-sectional area for a Gaussian transverse profile, and r_o is the laser spot size. In the following it is assumed that the pump amplitude A_o is a constant.

The x-ray radiation is given by the normalized vector potential

$$\mathbf{a}(\mathbf{r}, t) = [a(\mathbf{r}, t)/\sqrt{2}]\exp[i(k_z z - \omega t)]\hat{\mathbf{e}}_{\perp} + \text{c.c.}, \quad (2)$$

where $\lambda = 2\pi c/\omega$ is the x-ray wavelength and k_z is the complex axial wave number.

A. Thermal beam dispersion relation

Thermal effects associated with the electron beam play a critical role in the FEL interaction. The FEL dispersion relation including thermal effects is [13,15,16]

$$\begin{aligned} k_z^2 + k_{\perp}^2 - \frac{\omega^2}{c^2} &= -8f \frac{\nu}{r_b^2} \frac{a_o^2}{\gamma_o^3} \frac{\omega}{c} \frac{\omega_o}{c} \\ &\times \int_1^{\infty} \frac{d\gamma F_o(\gamma)}{[k_z + k_o - (\omega - \omega_o)/v_z + \mu k_{\perp}^2]^2}, \end{aligned} \quad (3)$$

where k_{\perp} is the transverse wave number, f is the filling factor, i.e., ratio of electron beam to radiation beam areas, $\nu = \omega_b^2 r_b^2/4c^2 = N_b r_e/\ell_b = I_b[A]/17000$ is Budker's parameter, $\omega_b = (4\pi q^2 n_b/m)^{1/2}$ is the electron beam plasma frequency, I_b is the beam current, $r_e = q^2/mc^2$ is the classical electron radius, ℓ_b is the electron bunch length, N_b is the number of electrons in a bunch, r_b is the electron beam radius, and $F_o(\gamma)$ is the electron distribution function.

The filling factor is a function of the interaction distance. In Eq. (3) $\mu = \gamma_{zo}^2 a_o^2/(2\gamma_o^2 \omega/c)$ is a correction term that arises from the transverse electron motion in the field of the pump laser. The resonant frequency is a function of k_{\perp} , and for $a_o^2 \ll 1$ is given by

$$\omega_R(k_{\perp}) = \omega_{R0}[1 - (\gamma_{zo}^2/\omega_{R0}^2)c^2 k_{\perp}^2], \quad (4)$$

where the resonant frequency for on-axis ($k_{\perp} = 0$) propagation is $\omega_{R0} = 4\gamma_{zo}^2 \omega_o = 4\gamma_o^2 \omega_o/(1 + a_o^2)$. The coherent radiation is emitted along the z axis inside a narrow cone with opening angle $\theta_k = k_{\perp}/k_z$. The range of allowed k_{\perp} 's, i.e., emission solid angle, is important in determining the incoherent and coherent x-ray power and is discussed in Sec. II E. A fully 3D dispersion relation, taking into account the finite electron beam radius, indicates that there is a limit on the range of transverse wave numbers [35]. In addition, the finite electron beam radius places a limit on k_{\perp} such that for the radiation to undergo at least one power e-fold, $k_{\perp} \leq (r_b/L_{go})k_z$.

1. Cold beam

For a cold beam the electron distribution function is $F_o(\gamma) = \delta(\gamma - \gamma_o)$ and the dispersion relation is given by $D_{\text{FEL}}(\mathbf{k}, \omega) = 0$, where

$$\begin{aligned} D_{\text{FEL}}(\mathbf{k}, \omega) &= \left[k_z - \frac{\omega}{c} \left(1 - \frac{c^2 k_{\perp}^2}{2\omega_{R0}^2} \right) \right] \\ &\times \left[k_z - \frac{\omega}{c} \left(1 + \frac{(\omega - \omega_{R0})}{2\gamma_{zo}^2 \omega_{R0}} - \frac{\mu c k_{\perp}^2}{\omega_{R0}} \right) \right]^2 \\ &+ (\Gamma_{go}/\sqrt{3})^3. \end{aligned} \quad (5)$$

For a cold beam, with $k_{\perp} = 0$ and $\omega = \omega_{R0}$, we find $k_z = \omega/c + \Delta k$, where $\Delta k = (1/\sqrt{3} - i)\Gamma_{go}/2$. However,

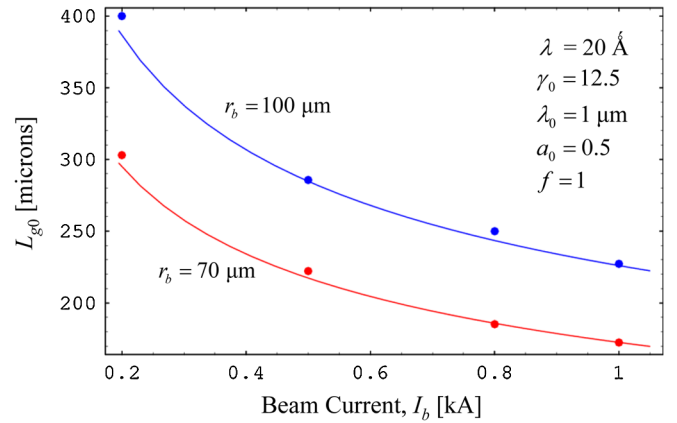


FIG. 2. (Color) X-ray ($\lambda = 20$ Å) power gain length L_{go} versus beam current for a cold electron beam with electron beam radius $r_b = 70$ μm (red) and $r_b = 100$ μm (blue). The curves are from Eq. (6) with $L_{go} = 1/\Gamma_{go}$ and the solid circles are from GENESIS simulations. The other parameters are $a_o = 0.5$, $\lambda_o = 1$ μm , and $E_b = 5.88$ MeV.

TABLE I. Parameters for a laser-pumped FEL.

Electron beam parameters	
Energy	$E_b = 5.88$ MeV ($\gamma_o = 12.5$)
Current	$I_b = 500$ A
Radius	$r_b = 70$ μ m
Energy spread limit	$\Delta\gamma/\gamma_o \leq \eta = 0.01\%$
Pump laser parameters	
Wavelength	$\lambda_o = 1$ μ m
Strength	$a_o = 0.5$
Spot size	$r_o = 400$ μ m
Rayleigh length	$Z_{R0} = 0.5$ m
Pulse duration	$\tau_L = 2L_{\text{sat}}/c = 23$ psec
X-ray parameters	
Wavelength	$\lambda = 20$ \AA
Spot size (at saturation)	$r_s = 70$ μ m
Rayleigh length (at saturation)	$Z_R = 7.7$ m
Power gain length	$L_{go} = 280$ μ m
Conversion efficiency	$\eta = 0.01\%$
Saturation length	$L_{\text{sat}} = 0.35$ cm
Saturated power	$P_{\text{sat}} = 300$ kW

to lowest order in the transverse wave number k_\perp and frequency detuning $\omega - \omega_{R0}$ parameters, the wave-number shift is $\Delta k = [\Gamma_{go}/(2\sqrt{3})]\{1 - 2(\varepsilon_1 - 2\varepsilon_2)/3 - i\sqrt{3}[1 - (\varepsilon_1 + \varepsilon_2)^2/9]\}$, where $\varepsilon_1 = (\omega_{R0}/c)(\sqrt{3}/\Gamma_{go}) \times (ck_\perp/\sqrt{2}\omega_{R0})^2$ and $\varepsilon_2 = (\omega_{R0}/c)(\sqrt{3}/\Gamma_{go}) \times (\omega - \omega_{R0})/(2\gamma_{zo}^2\omega_{R0})$. The power growth rate as a function of ω and k_\perp is

$$\Gamma_g(\omega, k_\perp) = \Gamma_{go}\{1 - [\omega - \omega_R(k_\perp)]^2/\Delta\omega^2\}, \quad (6)$$

where the peak growth rate is $\Gamma_{go} = (5.07/\gamma_o) \times [f\nu a_o^2/(r_b^2\lambda_o)]^{1/3}$, the power gain length is $L_{go} = 1/\Gamma_{go}$, and the linewidth associated with the power growth rate is $\Delta\omega/\omega_{R0} = (\lambda_o/L_{go})/2\pi$. As an example, the power gain length for x rays at $\lambda = 20$ \AA is shown in Fig. 2 for a cold electron beam as a function of beam current. The parameters for this plot are listed in Table I.

2. Thermal beam

For a thermal electron beam with distribution function $F_o(\gamma) = (\sqrt{\pi}\delta\gamma)^{-1} \exp[-(\gamma - \gamma_o)^2/\delta\gamma^2]$, the dispersion relation for $k_\perp = 0$ is

$$\Delta k = \frac{\lambda_o}{4\pi} \left(\frac{\Gamma_{go}}{\sqrt{3}}\right)^3 \frac{\gamma_o}{\delta\gamma} \times \int_{-\infty}^{\infty} \frac{dx \pi^{-1/2} x \exp(-x^2)}{\Delta k - 2k_o(\omega - \omega_{R0})/\omega_{R0} + 4k_o(\delta\gamma/\gamma_o)x}, \quad (7)$$

where $\delta\gamma/\gamma_o$ is the fractional energy spread. The dispersion relation can be written in the form

$$\xi = -\rho_o[1 + \{\xi + \xi_o\}Z(\xi + \xi_o)], \quad (8)$$

where $\xi = -(\gamma_o/\delta\gamma)\Delta k/4k_o$, $\xi_o = (\gamma_o/\delta\gamma) \times (\omega - \omega_{R0})/2\omega_{R0}$, $\Delta k = \Delta k_r - i\Gamma_g/2$, $\rho_o = 2.4 \times 10^{-5}(\lambda_o\Gamma_{go})^3(\gamma_o/\delta\gamma)^3$, $Z(\xi) \equiv \pi^{-1/2} \int_{-\infty}^{\infty} dx \exp(-x^2)/(x - \xi)$ is the plasma dispersion function, and gain occurs when the imaginary part of ξ is positive. In the cold beam limit $|\xi + \xi_o| \gg 1$ the dispersion relation reduces to the usual cubic equation with power growth rate given by Eq. (6) for $k_\perp = 0$ and $\xi_o = 0$.

The thermal dispersion relation can be analyzed in various limits. In the thermal beam limit $|\xi + \xi_o| < 1$ the dispersion relation reduces to [15]

$$\xi = -\rho_o\{1 + i\sqrt{\pi}(\xi + \xi_o) \exp[-(\xi + \xi_o)^2]\}, \quad (9)$$

where $Z(|\xi| < 1) = i\sqrt{\pi} \exp(-\xi^2)$. For $1 > |\xi_o| \gg |\xi|$ the imaginary part of ξ is $\xi_i = -\pi^{1/2}\rho_o\xi_o \exp(-\xi_o^2)$, where $\rho_o \ll 1$. The maximum growth rate occurs at $\xi_o = -1/\sqrt{2}$ and is given by [15,27]

$$\Gamma_g/\Gamma_{go} = 9.1 \times 10^{-4}(\lambda_o\Gamma_{go})^2(\gamma_o/\delta\gamma)^2. \quad (10)$$

Note that the thermal growth rate is inversely proportional to the square of the energy spread. The power growth rate at resonance ($\xi_o = 0$) in the thermal beam limit is

$$\Gamma_g/\Gamma_{go} = \frac{5.2 \times 10^{-8}(\lambda_o\Gamma_{go})^5(\gamma_o/\delta\gamma)^5}{1 + 1.8 \times 10^{-9}(\lambda_o\Gamma_{go})^6(\gamma_o/\delta\gamma)^6}. \quad (11)$$

In the extreme thermal limit $|\xi| \ll 1$, the power growth rate at resonance is given by

$$\Gamma_g/\Gamma_{go} = 5.2 \times 10^{-8}(\lambda_o\Gamma_{go})^5(\gamma_o/\delta\gamma)^5. \quad (12)$$

Figure 3 plots the normalized growth rate for x rays at $\lambda = 20$ \AA as a function of relative electron beam energy spread and detuning for the parameters listed in Table I. Figure 3 shows that, as the energy spread of the beam is increased up to $\delta\gamma/\gamma_o \sim 5 \times 10^{-4}$, the FEL interaction can be detuned to increase the growth rate relative to the resonant growth rate. For a given energy spread, the optimal detuning, i.e., maximum growth rate, occurs when the difference between the beam velocity and the phase velocity of the wave is equal to the thermal velocity spread of the beam. For $\delta\gamma/\gamma_o > 5 \times 10^{-4}$, the growth rate is vanishingly small regardless of detuning.

B. X-ray conversion efficiency

The saturated coherent power is $P_{\text{coh,sat}} = \eta N_b \gamma_o m c^2 / \tau_b$, where $\eta = P_{\text{coh,sat}}/P_b$ is the conversion efficiency and $P_b = N_b \gamma_o m c^2 / \tau_b = \nu \gamma_o m c^3 / r_e$ is the electron beam power. The conversion efficiency in the cold beam limit can be obtained by considering the difference between the electron beam energy before and after trapping in the ponderomotive potential [17]. The efficiency at saturation is $\eta = (2/\gamma_o)(\partial\gamma_o/\partial\beta_{zo})(\beta_{zo} - \beta_{\text{ph}})$, where β_{ph} is the normalized axial phase velocity of

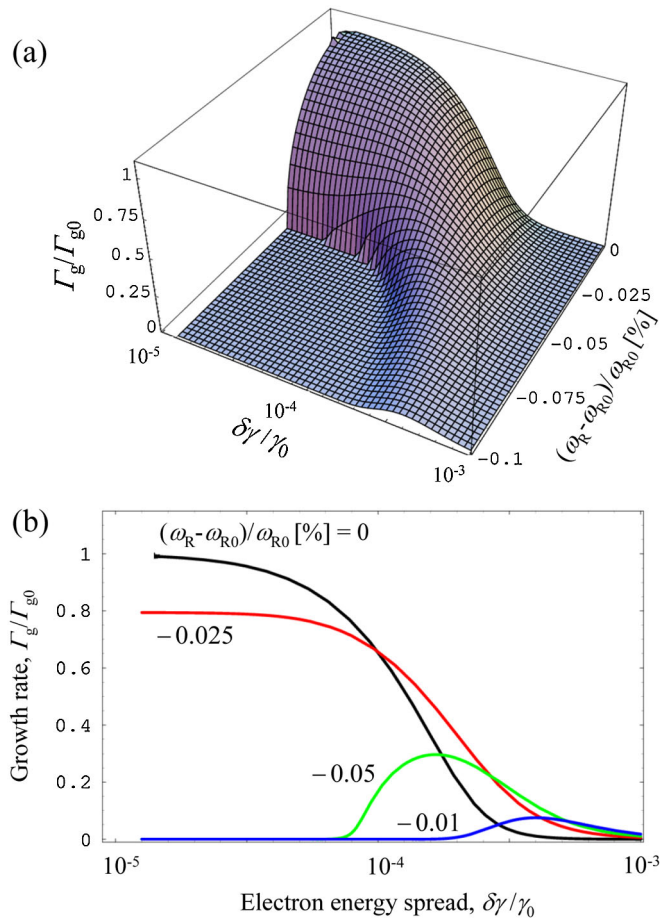


FIG. 3. (Color) (a) Surface plot of normalized x-ray growth rate Γ_g/Γ_{g0} from Eq. (8) versus fractional electron beam energy spread $\delta\gamma/\gamma_0$ and fractional detuning $(\omega - \omega_{R0})/\omega_{R0}$ for the parameters of the laser-pumped FEL of Table I. (b) Line plots of Γ_g/Γ_{g0} versus $\delta\gamma/\gamma_0$ for various values of detuning for the same data as shown in Fig. 3(a).

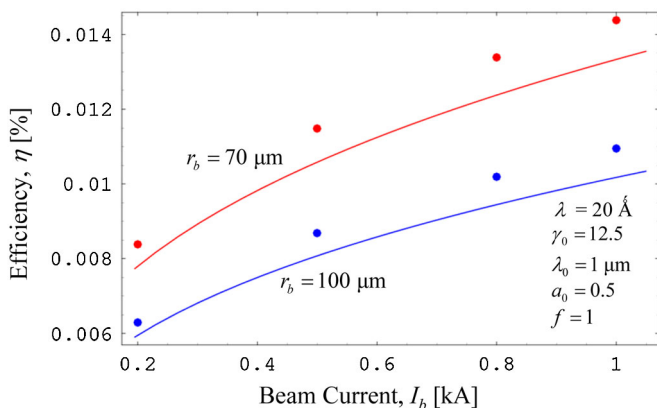


FIG. 4. (Color) X-ray conversion efficiency versus beam current for a cold electron beam, with electron beam radius $r_b = 70 \mu\text{m}$ (red) and $r_b = 100 \mu\text{m}$ (blue). The curves are from Eq. (13) and the solid circles are from GENESIS simulations. The parameters are the same as in Fig. 2.

the ponderomotive wave. From the dispersion relation the phase velocity is found to be $v_{\text{ph}}/c = (\omega - \omega_o)/c(k_z + k_o) = \beta_{z_o} - \text{Re}(\Delta k)/k_z + k_{\perp}^2/(2k_z^2)$. The conversion efficiency at saturation, for $k_{\perp} = 0$, is [17]

$$\eta = 0.023(\lambda_o/L_{g0}). \quad (13)$$

The expression in Eq. (13) assumes that all the electrons contributing to the growth of the radiation become trapped in the ponderomotive buckets at saturation; i.e., the trapping fraction is 100%. The x-ray conversion efficiency plotted as a function of beam current is shown in Fig. 4 for a cold electron beam along with results from GENESIS simulations. The parameters for this plot are listed in Table I. There is good agreement between theory and simulations.

C. Validity of classical description

The classical description is valid if the electron momentum recoil is somewhat less than the electron thermal momentum spread. In the beam frame (indicated by a prime on the variables) this condition is $\hbar k' \ll m\Delta v'$ and in the laboratory frame it can be written as [36–38]

$$\frac{2\gamma_o}{\sqrt{1+a_o^2}} \left(\frac{\Delta\gamma}{\gamma_o} \right) \left(\frac{\lambda}{\lambda_c} \right) > 1, \quad (14)$$

where $\lambda_c = 2\pi\hbar/mc = 0.024 \text{ \AA}$ is the Compton wavelength, $\Delta\gamma/\gamma_o = \gamma_o^2(1+a_o^2)^{-1}\Delta v_z/c$ is the fractional energy spread, and Δv_z is the axial velocity spread. A more detailed analysis performed in [36,37] shows that the inequality in Eq. (14) is more accurately given by $\eta\gamma_o(\lambda/\lambda_c) > 0.4$. In the example presented in this paper $\eta\gamma_o(\lambda/\lambda_c) \approx 1$ and quantum effects reduce the classical growth rate by $\sim 10\%$, see Fig. 1 in Ref. [37].

D. Electron beam quality requirements

The beam quality requirements for a laser-pumped x-ray FEL are extremely challenging [31]. For high gain and efficiency the electrons must remain in phase with the ponderomotive (trapping) wave. As a result the interaction is sensitive to an axial electron velocity spread. A spread in axial electron velocity Δv_z can result in phase mixing which would reduce the gain and efficiency. The electron beam can be considered cold, i.e., monoenergetic, provided $\Delta v_z L_{g0}/c \ll \lambda$, which can be written in terms of the fractional energy spread $\Delta\gamma/\gamma \ll \lambda_o/4L_{g0} \approx 10\eta$. The energy spread on the beam consists of several contributions. These contributions include: (i) intrinsic energy spread, (ii) transverse and longitudinal emittance, (iii) space charge, (iv) pump laser linewidth, and (v) pump laser field gradients. The overall energy spread is

$$\frac{\Delta\gamma}{\gamma_o} = \left(\frac{\Delta\gamma}{\gamma_o}\right)_{\text{intrinsic}} + \left(\frac{\Delta\gamma}{\gamma_o}\right)_{\perp,\text{emit}} + \left(\frac{\Delta\gamma}{\gamma_o}\right)_{z,\text{emit}} + \left(\frac{\Delta\gamma}{\gamma_o}\right)_{\text{space charge}} + \left(\frac{\Delta\gamma}{\gamma_o}\right)_{\text{pump linewidth}} + \left(\frac{\Delta\gamma}{\gamma_o}\right)_{\text{pump grad}}, \quad (15)$$

where $(\Delta\gamma/\gamma_o)_{\perp,\text{emit}} = \varepsilon_n^2/2r_b^2 \sim 2 \times 10^{-4}$, ($\varepsilon_n = 1$ mm mrad, $r_b = 50$ μm), $(\Delta\gamma/\gamma_o)_{z,\text{emit}} = \varepsilon_{n,z}^*/(\tau_b E_b) \sim 2.5 \times 10^{-4}$ ($\varepsilon_{n,z}^* = 25$ keV-psec, $\tau_b = 10$ psec, and $E_b = 10$ MeV), $(\Delta\gamma/\gamma_o)_{\text{space charge}} = \nu/\gamma_o$, $(\Delta\gamma/\gamma_o)_{\text{pump linewidth}} = \delta\lambda/2\lambda_o < 10^{-4}$. Here, ε_n is the normalized transverse emittance and $\varepsilon_{n,z}^*$ is the normalized axial emittance [39]. The energy spread contribution due to space charge leads to an energy shear which can, in principle, be eliminated or substantially reduced by creating the electron beam with an appropriate radial energy shear.

The electron beam brightness $B_n = 2I_b/(\pi^2 \varepsilon_n^2)$ is a measure of beam quality [39]. At the cathode the normalized brightness can be expressed as $B_n = J_c mc^2/(2\pi k_B T_c)$, where J_c is the current density at the cathode and T_c is the cathode temperature. For a photocathode with $k_B T_c = 0.1$ eV and $J_c = 100$ A/cm², the brightness is $B_n \sim 10^8$ A/(cm-rad)². The brightness needed in a laser-pumped x-ray FEL is about an order of magnitude higher, i.e., $\geq 10^9$ A/(cm-rad)². An axial magnetic field may be necessary to guide the electron beam through the interaction region. The magnetic field required for a matched, i.e., constant radius, electron beam is B [kG] = $(4.7/r_b$ [cm]) $(\nu/\gamma_o)^{1/2} \sim 30$ kG. For the parameters considered here the electron beam undergoes less than a complete gyrorotation in the interaction region and therefore the effect of the magnetic field on the gain process is expected to be negligible.

E. Radiation solid angle

The transition from spontaneous to coherent radiation is critically dependent on the angular distribution of the waves. Waves with finite k_{\perp} have a propagation angle $\theta_k = k_{\perp}/k_z$ with respect to the z axis. The peak growth rate is independent of k_{\perp} for waves propagating in the near-forward direction as indicated in Eq. (6). However, as k_{\perp} increases the resonant frequency $\omega = \omega_R(k_{\perp})$ decreases as indicated schematically in Fig. 5. The minimum propagation angle is $\theta_{k,\text{min}} = \theta_D = \lambda/\pi r_s$ where θ_D is the diffraction angle, r_s is the radial dimension of the radiation beam, and $k_{\perp,\text{min}} = 2/r_s$. In general, however, k_{\perp} can be significantly greater than $k_{\perp,\text{min}}$. From the power gain expression in Eq. (6), the maximum transverse wave number, for gain at resonance ($\omega = \omega_{R0}$), is given by

$$k_{\perp,\text{max}} = \theta_{k,\text{max}} k_z \approx \frac{3}{\sqrt{\pi}} \left(\frac{\lambda}{L_{go}}\right)^{1/2} k_z. \quad (16)$$

The ratio of the maximum to minimum transverse wave numbers is $k_{\perp,\text{max}}/k_{\perp,\text{min}} \approx 3(Z_R/L_{go})^{1/2}$, where $Z_R =$

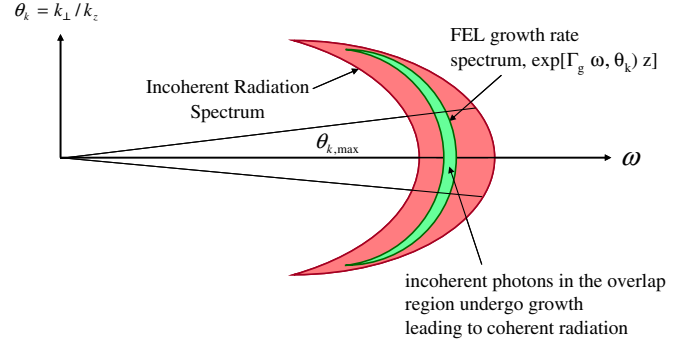


FIG. 5. (Color) Schematic diagram of the incoherent (spontaneous) and coherent (growth rate) spectrum in the $(\omega, k_{\perp}/k_z)$ plane showing the region of overlap. The red area corresponds to the region of incoherent emission of radiation from the electron beam interacting with the pump laser. The green area indicates the growth rate spectral region in which the radiation grows exponentially.

$\pi r_s^2/\lambda$ is the Rayleigh range associated with the x rays. For a laser-pumped FEL, $Z_R \gg L_{go}$, while for an optically guided FEL amplifier, $Z_R \approx L_{go}$. Other processes, such as the electron transverse wobble and betatron oscillations, can also limit the range of transverse wave numbers.

The solid angle associated with the radiation beam is $\Delta\Omega_k = \pi\theta_{k,\text{max}}^2$, where $\theta_{k,\text{max}} = k_{\perp,\text{max}}/k_z$. The spontaneous (incoherent) radiation [40–42] is directed into a forward cone with angle $\theta_{\text{incoh}} \approx 1/\gamma_{zo}$ which is typically much greater than $\theta_{k,\text{max}}$. In the start-up regime the propagation angle $\theta_{k,\text{max}}$ determines the portion of the spontaneous power that is within the gain spectrum and amplified as shown schematically in Fig. 5.

F. Effects of a finite spot-size laser pump

The finite spot size of the pump laser affects the FEL interaction in a number of ways. Transverse gradients in the pump laser result in a resonant frequency spread across the beam and diffraction leads to both amplitude and phase changes.

Transverse pump laser effects can be significantly reduced by the addition of higher-order Laguerre-Gaussian modes. For a laser pump undergoing diffractive spreading and which includes the fundamental with amplitude a_0 and the next high-order mode with amplitude a_1 , the transverse pump field is given by

$$\mathbf{a}_{o\perp}(\mathbf{r}, t) = (a_o/\sqrt{2})\{1 + [1 - 2(r^2/r_o^2)]\rho \exp[2i\theta_g(z)]\} \times F(r, z, t) \exp[-i(k_o z + \omega_o t)]\hat{\mathbf{e}}_{\perp} + \text{c.c.},$$

where $F(r, z, t) = G(z + v_g t)[r_o/r_L(z)] \exp[-ik_o r^2/2R_c(z)] \exp[i\theta_g(z)] \exp[-r^2/r_L^2(z)]$, $\rho = a_1/a_0$ is the ratio of the higher-order mode amplitude to the fundamental, $r_L(z) = r_o(1 + z^2/Z_{R0}^2)^{1/2}$ is the spot size, $Z_{R0} = \pi r_o^2/\lambda_o$ is the Rayleigh range associated with the pump laser,

$R_c(z) = z + Z_{R0}^2/z$ is wave front radius of curvature, and $\theta_g = \tan^{-1}(z/Z_{R0})$ is the Gouy phase. In addition, there is a small axial pump laser field component of order λ_o/r_o times the transverse component. The function $G(z + v_g t)$ defines the envelope of the pump laser and v_g is the group velocity. The group velocity is a function of the mode number m and is given by $v_g \approx c[1 - (1 + 2m)/(k_o Z_{R0})]$ near the axis, for $|z| \ll Z_{R0}$. The envelope of the fundamental mode and the higher-order modes separate by much less than a wavelength λ_o if the interaction length is short compared to the Rayleigh length, $|z| \ll (\pi/m)Z_{R0}$ where $m = 1, 2, 3, \dots$. Hence, we can use the group velocity of the fundamental mode to describe the envelope dynamics.

Taking the interaction length to be small compared to the Rayleigh length, $|z| \ll Z_{R0}$, and a_o and a_1 to be real we find that to order r^2 , $\mathbf{a}_{o\perp} \cdot \mathbf{a}_{o\perp} = a_o^2(1 + \rho)[1 + \rho - 2(1 + 3\rho)r^2/r_o^2]$ and the radial variation can be eliminated to order r^2 by setting $\rho = -1/3$. Hence, transverse gradients in the pump laser can be reduced by appropriately including additional modes. Figure 6(a) plots the transverse intensity profile for a two-mode pump laser with mode amplitude ratio $\rho = -1/3$ and for a fundamental Gaussian mode with identical power (dashed curve). The addition of a higher-order mode flattens the intensity profile near the axis and reduces the resulting resonant frequency spread.

We numerically solve the fully relativistic, 3D equations of motion to obtain particle trajectories in the pump field, including the axial component, and calculate the resulting resonant frequency spread. Figure 6(b) plots the fractional resonant frequency spread versus propagation distance for an electron beam with $\gamma_o = 12.5$, $r_b = 70 \mu\text{m}$, and beam emittance $\varepsilon_n = 1 \text{ mm mrad}$. The fractional resonant frequency spread is calculated as $\langle (\omega_R - \omega_{R0})/\omega_{R0} \rangle = \langle [a_o^2(0) - a_o^2(r)]/[1 + a_o^2(r)] \rangle$, where r is the radial position of a particle and $\langle \rangle$ denotes an average over particles. The longitudinal profile is taken to have the form $G(\xi) = (1/2)\{\tanh[10^3 k_o(\xi - z_o)] + 1\}$. The factor 10^3 in this expression is arbitrarily chosen to represent the sharp rise at the front of the pump laser pulse. For a fundamental Gaussian pump, the resonant frequency spread is $\sim 1\%$, which is much greater than the x-ray FEL efficiency. However, the addition of a single higher-order mode reduces the frequency spread by more than 2 orders of magnitude to $\sim 8 \times 10^{-3}\%$. For the parameters of routine, the Rayleigh range ($\sim 50 \text{ cm}$) is much greater than the interaction length ($\sim 0.35 \text{ cm}$). The on-axis vector potential of the pump laser, given by $a_0(z) = a_0(0)/(1 + z^2/Z_{R0}^2)^{1/2}$, decreases by $\sim 10^{-5}$ due to diffraction, and the electron beam radius, given by $r_b(z) = r_b(0)\{1 + \varepsilon_n^2 z^2/[\gamma_o^2 r_b^4(0)]\}^{1/2}$, increases by $< 1\%$ due to emittance over the interaction length. Both of these factors do not appreciably affect the resonant frequency spread as shown by Fig. 6(b). In principle, the resonant frequency

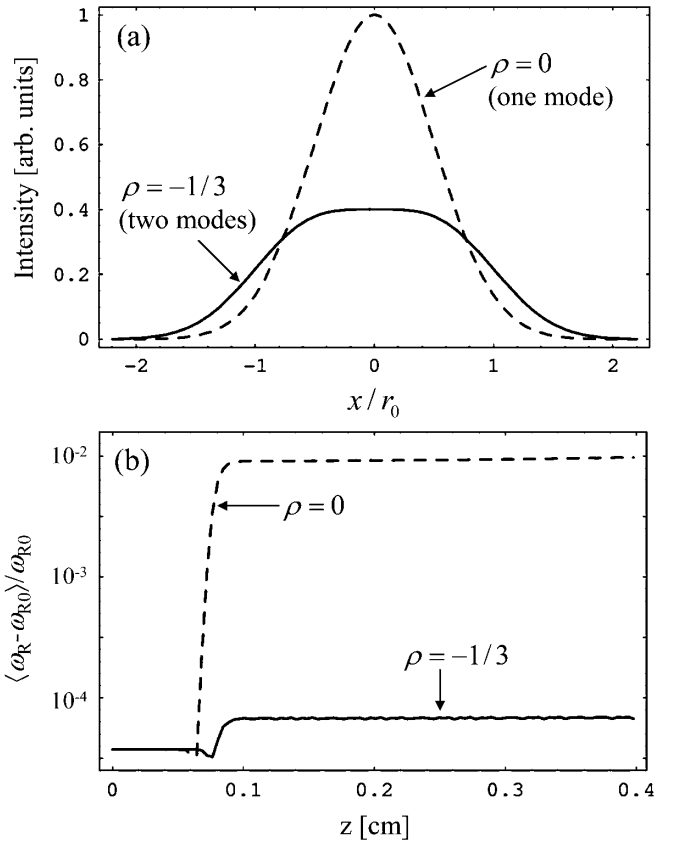


FIG. 6. Transverse gradients in the pump laser can be significantly reduced by the addition of higher-order Laguerre-Gaussian modes. (a) Intensity versus transverse position for a pump lasers with $\rho = 0$ (fundamental Gaussian) and $\rho = -1/3$ (two modes) with equal power, where $\rho = a_1/a_0$ is the ratio of mode amplitudes. The fundamental mode is characterized by $a_0 = 0.5$, $r_0 = 400 \mu\text{m}$, $\lambda_0 = 1 \mu\text{m}$, and $Z_R = 50 \text{ cm}$. (b) Resonant frequency spread versus propagation distance for an electron beam with $\gamma_o = 12.5$, $r_b = 70 \mu\text{m}$, and beam emittance $\varepsilon_n = 1 \text{ mm mrad}$ interaction with a pump laser with $\rho = 0$ and $\rho = -1/3$. The inclusion of a higher-order mode reduces the resonant fractional frequency spread by more than 2 orders of magnitude, to $\sim 8 \times 10^{-3}\%$.

spread can be further reduced by the inclusion of additional higher-order modes. In the analysis and simulations that follow, we assume that the transverse gradients in the pump field can be neglected.

III. TRANSITION FROM INCOHERENT TO COHERENT RADIATION

The discrete nature of the electron beam interacting with the pump laser field leads to the generation of spontaneous (inco radiation that can be subsequently amplified [21–26]. During amplification, however, there is an increase in the coherence of the radiation.

The wave equation governing the x-ray generation is $(\nabla^2 - c^{-2}\partial^2/\partial t^2)\mathbf{E}(\mathbf{r}, t) = 4\pi c^{-2}g(z)\partial\mathbf{J}(\mathbf{r}, t)/\partial t + 4\pi g(z)\nabla\rho(\mathbf{r}, t)$, where the field and current density are

$\mathbf{E}(\mathbf{r}, t), \mathbf{J}(\mathbf{r}, t) = [E(\mathbf{r}, t), J(\mathbf{r}, t)]\hat{\mathbf{e}}_{\perp} + \text{c.c.}$, $\rho(\mathbf{r}, t)$ is the charge density, and $g(z) = 1$ for $0 \leq z \leq \bar{z}$ defines the interaction region and is zero otherwise. The driving cur-

rent density consists of a coherent and an incoherent (discrete) component

$$\mathbf{J}(x, y, z, t) = q \sum_{i=1}^{N_b} \tilde{\mathbf{v}}_i(t) \delta[x - \tilde{x}_i(t)] \delta[y - \tilde{y}_i(t)] \delta[z - \tilde{z}_i(t)] = \mathbf{J}_{\text{coh}}(\mathbf{r}, t) + q \sum_{i=1}^N \tilde{\mathbf{v}}_i^{(o)}(\mathbf{r}_o, \mathbf{v}_o, t) \delta[\mathbf{r} - \tilde{\mathbf{r}}_i^{(o)}(t)], \quad (17)$$

where $\tilde{\mathbf{r}}^{(o)}(t), \tilde{\mathbf{v}}_i^{(o)}(t)$ \tilde{\mathbf{1票}^{(o)} = (-c\mathbf{a}_o/\gamma_o, v_{zo}), $\mathbf{J}_{\text{coh}}(\mathbf{r}, t)$ is the coherent current density which is responsible for the FEL interaction, and the summation term in Eq. (17) is responsible for spontaneous emission. Substituting the current density, Eq. (17), into the wave equation and Fourier transforming the spatial and temporal variables we obtain

$$D(\mathbf{k}, \omega) \hat{E}(k_x, k_y, k_z, \omega) = \frac{1}{8\pi^2} \left(\frac{4\pi q}{c} \right) \frac{a_o}{\sqrt{2}} \frac{i}{\gamma_o} \bar{z} \exp[iK(k_z, \omega)\bar{z}/2] \left(\frac{\sin[K(k_z, \omega)\bar{z}/2]}{K(k_z, \omega)\bar{z}/2} \right) \sum_{i=1}^{N_b} \exp(i\chi_{o,i}), \quad (18)$$

where $K(k_z, \omega) = (\omega - \omega_o)/v_{zo} - (k_z + k_o)$, $\chi_{o,i} = -k_x x_{o,i} - k_y y_{o,i} + (\omega - \omega_o)t_{o,i}$, and the charge density has been neglected [23]. In obtaining Eq. (18) harmonics are neglected since we assumed $k_{\perp} |\delta x| \ll 1$, where $|\delta x| = a_o/(2\gamma_o k_o)$ is the magnitude of the electron transverse wiggle motion in the pump laser.

The function $D(\mathbf{k}, \omega)$ is given by

$$D(\mathbf{k}, \omega) = - \frac{D_{\text{FEL}}(\mathbf{k}, \omega)}{\{k_z - (\omega/c)[1 + (\omega - \omega_{R0})/(2\gamma_{zo}^2 \omega_{R0})]\}^2} = - \frac{[k_z - k_1(k_{\perp}, \) 19)$$

where the roots of the dispersion relation are denoted by k_1, k_2, k_3 , and k_1 denotes the growing root32009) the growing rootail. Solving Eq. (18) for the field associated the growing root, i.e., integrating around the pole at $k_z = k_1(k_{.) 2009) we obtain$

\hat{E}(k_{, 2009) \hat{E}(k_{\perp}, z, \omega) = \frac{1}{2(\这些数据39) \frac} \frac{q}{c} \frac{a_o}{\gamma_o} \bar{z} \exp(iK_1 \bar{z}/2) \left(\frac{\sin(K_1 \bar{z}/2)}{K_1 \bar{z}/2} \right) G(k_1, k_{\perp}, \omega) \exp[ik_1(k_{\馁 } z) \sum_{i=1}^{N_b} \text{exp}(i\chi_{o,i}),) \quad (20)

K_1 = K - \omega_o)/v_z< 2009) - (k_1 + k_o) = [\omega - \omega_{R0}(1 - \gamma_{, 2009) \omega_{R0}^2)/2c\gamma_{zo}^2}] and $G(k_1, k_{\perp}, \omega) = \{[kutzer + k_o - (\omega - \omega_o)/v_{zo}]^2\}/[ryk_1 - k_2umbs, \omega)\} [нде 2009) 2009)$

The intensity is given by $I(r, z, t) = (c/2\pi) \langle E(r, tack) E'*(oltutedots irrational $\langle \rangle$ denotes an average over electrons. If the electrons are initially randomly distributed, we use the fact that $\langle \sum_{i=1}^{N_b} \text{exp}(i\chi_{o,i}) \sum_{j=1}^{N_b} \text{exp}(-i\chi_{o,j}) \rangle = N_b$ and obtain$

$$\langle \hat{E}(r, z, \omega) \hat{E}^*(r, z, \omega) \rangle = \frac{1}{4\pi} \frac{q^2}{c^2} \frac{a_o^2}{\gamma_o^2} N_b \left| \int_0^{\infty} k_{\perp} dk_{\perp} z \exp\left(i \frac{K_1 z}{2}\right) \left(\frac{\sin(K_1 z/2)}{K_1 z/2} \right) G(k_1, k_{\perp}, \omega) J_o(k_{\perp} r) \exp[ik_1(k_{\perp}, \omega)z] \right|^2, \quad (21)$$

where we have set $\bar{z} = z$. The spectral power, defined by

$$\begin{aligned} \frac{d^2 \hat{P}}{d\omega} &= \int d\Omega_k \left(\frac{d^2 \hat{P}}{d\omega d\Omega_k} \right) \\ &= \frac{c}{\tau_b} \int_0^{\infty} r dr \langle \hat{E}(r, z, \omega) \hat{E}^*(r, z, \omega) \rangle, \end{aligned} \quad (22)$$

is given by\begin{aligned} \frac{d^2 \hat{P}}{d\omega d\Omega_k} &= 8\nu \gamma_o^2 m c^2 \left(\frac{z}{\lambda_o} \right)^2 \left(\frac{a_o}{1 + a_o^2} \right)^2 |\exp(iK_1 z/2)|^2 \\ &\times \left| \frac{\sin(K_1 z/2)}{K_1 z/2} \right|^2 |G(k_1, k_{\perp}, \omega)|^2 \\ &\times |\exp[ik_1(k_{\perp}, \omega)z]|^2, \end{aligned} \quad (23)

where $k_{\perp} dk_{\perp} = (k_z^2/2\pi) d\Omega_k$, $d\Omega_k$ is the differential solid

angle associated with the wave vector, and the relation $\int_0^{\infty} r dr J_o(k_{\perp} r) J_o(k'_{\perp} r) = \delta(k_{\perp} k'_{\perp})/k_{\perp}$ was used.

A. Incoherent radiation

The spectral brightness in the absence of the FEL interaction is the spontaneous (incoherentatria) spectral brightness and is obtained from Eq. (23) wher 2009) by setting k_ = (\omega/c) \times因为没有 c^2 k_{\perp}^2/2\omega_{R0}^2, together with $|\exp(iK_1 z/2)|^2 = |G(k_1, k_{\perp}, \omega)|^2 = |\exp[ik_1(k_{\perp}, \omega)z]|^2 = 1$. The incoherent spectral brightness is

$$\left(\frac{d^2 \hat{P}_{\text{incoh}}}{d\omega d\Omega_k} \right) = 8\nu \gamma_o^2 m c^2 \left(\frac{z}{\lambda_o} \right)^2 \left(\frac{a_o}{1 + a_o^2} \right)^2 \left| \frac{\sin(K_1 z/2)}{K_1 z/2} \right|^2. \quad (24)$$

The incoherent power radiated by the electron bunch per

unit solid angle is

$$\begin{aligned} \frac{dP_{\text{incoh}}}{d\Omega_k} &= \int_0^\infty d\omega \left(\frac{d^2 \hat{P}_{\text{incoh}}}{d\omega d\Omega_k} \right) \\ &= 4\pi\gamma_o^2 \frac{\nu mc^3}{\lambda} \frac{z}{\lambda_o} \left(\frac{a_o}{1+a_o^2} \right)^2. \end{aligned} \quad (25)$$

The incoherent power within the solid angle $\Delta\Omega_{\text{incoh}}$ is

$$P_{\text{incoh}}(z) = 16\pi\gamma_o^3 \frac{a_o^2}{(1+a_o^2)^3} \frac{r_e}{\lambda_o} \frac{z}{\lambda_o} \Delta\Omega_{\text{incoh}} P_b, \quad (26)$$

where $\Delta\Omega_{\text{incoh}} \leq \pi/\gamma_{zo}^2$ is the solid angle associated with the incoherent radiation and $P_b = \nu\gamma_o mc^3/r_e$ is the electron beam power.

B. Coherent radiation

A small portion of the spontaneous radiation spectrum overlaps the gain spectrum and is amplified as depicted in Fig. 5. The coherently amplified portion of the spectrum is determined by the relative linewidths of the spontaneous and gain spectra, as well as the range of amplified transverse wave numbers k_\perp given by Eq. (16). The fractional linewidths associated with the coherent and incoherent (spontaneous) power spectrum are, respectively,

$$\delta\omega_{\text{coh}}(z)/\omega_{R0} = (1/2\pi)(\lambda_o/L_{go})\sqrt{L_{go}/z}, \quad (27a)$$

and

$$\delta\omega_{\text{incoh}}(z)/\omega_{R0} = (1/2)(\lambda_o/z). \quad (27b)$$

The ratio of the linewidths is $\delta\omega_{\text{coh}}/\delta\omega_{\text{incoh}} = (1/\pi) \times \sqrt{z/L_{go}}$ which implies that for interaction distances less than $\sim 10L_{go}$, the coherent power spectrum is narrower than the spontaneous spectrum. For $z > L_{go}$, we find that $|\exp(iK_1 z/2)|^2 |\sin(K_1 z/2)/(K_1 z/2)|^2 \approx (2L_{go}/z)^2$, and the coherent power spectral brightness in Eq. (23) is

$$\begin{aligned} \frac{d^2 \hat{P}_{\text{coh}}}{d\omega d\Omega_k} &= (32/9)\nu\gamma_o^2 mc^2 \left(\frac{z}{\lambda_o} \right)^2 \left(\frac{a_o}{1+a_o^2} \right)^2 \left(\frac{L_{go}}{z} \right)^2 \\ &\times \exp[\Gamma_g(\omega, k_\perp)z], \end{aligned} \quad (28)$$

where we used $|G(k_1, k_\perp, \omega)|^2 = 1/9$, i.e., 1/9 of the incoherent power is available for gain.

Using the power growth rate spectrum in well-defined interaction distances, the coherent power spectrum is narrower than the spontaneous spectrum. For $z > L_{go}$, we find that $|\exp(iK_1 z/2)|^2 |\sin(K_1 z/2)/(K_1 z/2)|^2 \approx (2L_{go}/z)^2$, and the coherent power spectral brightness in Eq. (23) is

$$\begin{aligned} \frac{dP_{\text{coh}}}{d\Omega_k} &= 6.3\nu\gamma_o^2 mc^2 \left(\frac{z}{\lambda_o} \right)^2 \left(\frac{a_o}{1+a_o^2} \right)^2 \left(\frac{L_{go}}{z} \right)^2 \left(\Delta\omega \sqrt{\frac{L_{go}}{z}} \right) \\ &\times \exp(\Gamma_{go}z), \end{aligned} \quad (29)$$

where $\Delta\omega/\omega_{R0} = (\lambda_o/L_{go})/2\pi$.

The coherent radiation beam is confined to a narrow forward cone with solid angle $\Delta\Omega_k = \pi\theta_{k,\text{max}}^2$, where $\theta_{k,\text{max}}$ is given by Eq. (16). The incoherent radiation, on

the other hand, is confined to a cone angle $\theta_{\text{incoh}} \approx 1/\gamma_{zo} > \theta_{k,\text{max}}$.

The integration over solid angle in Eq. (29) can be approximated by evaluating the integrand at $k_\perp = 0$ and multiplying by the solid angle $\Delta\Omega_k$. The coherent power is given by

$$\begin{aligned} P_{\text{coh}}(z) &= 25\gamma_o^3 \frac{a_o^2}{(1+a_o^2)^3} \left(\frac{L_{go}}{\lambda_o} \right) \left(\frac{r_e}{\lambda_o} \right) \\ &\times \left(\frac{L_{go}}{z} \right)^{1/2} \Delta\Omega_k P_b \exp(z/L_{go}). \end{aligned} \quad (30)$$

The coherent power in Eq. (30) will be compared with GENESIS simulations in the x-ray regime.

To compare the expression for the coherent power in Eq. (30) with those obtained for a conventional wiggler-based FEL, we consider the case where the interaction distance is much greater than a Rayleigh length, but shorter than the saturation length, $L_{\text{sat}} > z \gg Z_R$. In this case the propagation angle is equal to the diffraction angle, i.e., $\theta_k = \theta_D$, and the coherent power from Eq. (30) becomes

$$\begin{aligned} P_{\text{coh}}(z \gg Z_R) &= 0.01\eta\gamma_o mc^2 \left(\frac{z}{L_{go}} \right)^2 \left(\frac{r_b^2/r_s^2}{f} \right) \delta\omega_{\text{coh}}(z) \\ &\times \exp(z/L_{go}), \end{aligned} \quad (31)$$

where

$$\delta\omega_{\text{coh}}(z)/\omega_{R0} = (\Delta\omega/\omega_{R0})\sqrt{L_{go}/z} =$$

$6.9\eta\sqrt{L_{go}/z}$, $\eta = 0.023(\lambda_o/L_{go})$ is the conversion efficiency, and f is the filling factor. The coherent power in this limit, given by Eq. (31), is similar in form to that given in [21,23,24]. The ratio of the coherent power to the incoherent power for the same solid angle and for $z > L_{go}$ is

$$\begin{aligned} \left(\frac{P_{\text{coh}}}{P_{\text{incoh}}} \right)_{\Delta\Omega_k} &= 1.6 \left(\frac{L_{go}}{z} \right)^2 \frac{\delta\omega_{\text{coh}}(z)}{\delta\omega_{\text{incoh}}(z)} \exp(z/L_g) \\ &= \frac{1}{2} \left(\frac{L_{go}}{z} \right)^{3/2} \exp(z/L_{go}). \end{aligned} \quad (32)$$

C. Saturation length and linewidth

The saturation length for the coherent radiation can be obtained by setting P_{coh} in Eq. (30) equal to the conversion efficiency times the electron beam power, ηP_b , where η is given by Eq. (13). The number of power gain lengths at saturation, $N_{\text{sat}} = L_{\text{sat}}/L_{go}$, is given by

$$\begin{aligned} N_{\text{sat}}^{-1/2} \exp(N_{\text{sat}}) &= 9.2 \times 10^{-4} \left(\frac{\lambda_o}{L_{go}} \right)^2 \left(\frac{\lambda_o}{r_e} \right) \frac{(1+a_o^2)^3}{a_o^2} \\ &\times \frac{1}{\gamma_o^3 \Delta\Omega_k}. \end{aligned} \quad (33)$$

The fractional linewidth associated with the coherent radiation, for $k_\perp \sim 0$, at saturation is

$$\frac{\delta\omega_{\text{coh}}}{\omega_{R0}} = N_{\text{sat}}^{-1/2} \frac{\Delta\omega}{\omega_{R0}} = \frac{N_{\text{sat}}^{-1/2}}{2\pi} \frac{\lambda_o}{L_{go}}. \quad (34)$$

There is an additional contribution to the linewidth due to the finite transverse wave number, k_{\perp} , spectrum which is given by $\gamma_{zo}^2 \theta_k^2$, as indicated in Eq. (4).

IV. COMPARISON OF THEORY WITH SIMULATIONS

In this section we compare the analytical result for the coherent power, Eq. (30), with the simulation results from GENESIS [34]. GENESIS simulates the conventional wiggler-based FEL amplifier, including start-up. In using GENESIS to simulate the laser-pumped FEL, the wiggler period in GENESIS is set equal to twice the pump laser wavelength $\lambda_w = \lambda_o/2 = 0.5 \mu\text{m}$, and the wiggler transverse gradients are removed. Besides GENESIS there are other FEL simulation codes that can be used to simulate the FEL start-up physics [43]. Before discussing an example of an x-ray laser-pumped FEL it is useful to consider the application of the theory to a conventional FEL operating in the x-ray regime. For this comparison we use the Linac Coherent Light Source (LCLS) FEL at SLAC [1].

A. Wiggler-based x-ray FEL

The parameters of the LCLS FEL operating at 15 \AA are given in Table II. In the GENESIS simulations, we use a circularly polarized wiggler and a cold electron beam to make a comparison with theory. The wiggler strength parameter is therefore smaller by a factor of $\sqrt{2}$ than the actual value used in the original LCLS design [1]. Figure 7

TABLE II. Parameters for LCLS FEL. Note that the actual LCLS wiggler is linearly polarized with $a_w = 3.7$.

Electron beam parameters	
Energy	$E_b = 4.52 \text{ GeV}$ ($\gamma_o = 8.9 \times 10^3$)
Current	$I_b = 3.4 \text{ kA}$
Radius	$r_b = 110 \mu\text{m}$
Energy spread limit	$\Delta\gamma/\gamma_o \leq \eta = 0.08\%$
Wiggler (circular) parameters	
Period	$\lambda_w = 3 \text{ cm}$
Strength	$a_w = 2.62$
X-ray parameters	
Wavelength	$\lambda = 15 \text{ \AA}$
Spot size (at saturation)	$r_s = 140 \mu\text{m}$
Rayleigh length (at saturation)	$Z_R = 42 \text{ m}$
Power gain length	$L_{go} = 2 \text{ m}$
Conversion efficiency	$\eta = 0.08\%$
Saturation length	$L_{\text{sat}} = 28 \text{ m}$
Saturated power	$P_{\text{sat}} = 12.5 \text{ GW}$

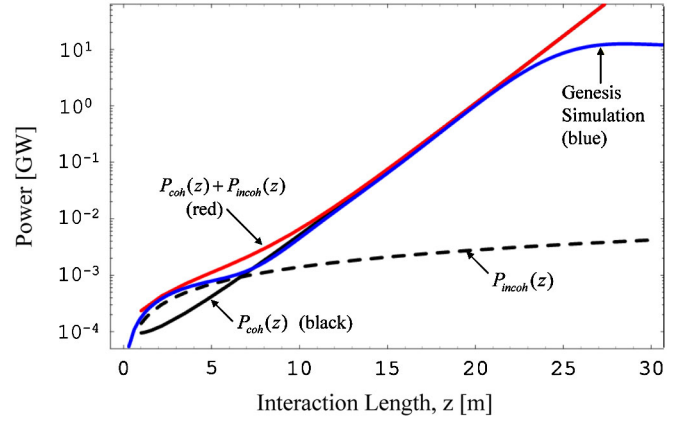


FIG. 7. (Color) Power versus interaction length for the LCLS FEL (cold beam) with parameters listed in Table II. Curves denote coherent power (solid black), incoherent power (dashed), total theoretical power (red), and the result of a GENESIS simulation (blue). The theoretical efficiency is $\eta = 0.046(\lambda_w/L_{go}) = 0.07\%$. The efficiency observed in the GENESIS simulation is 0.08%.

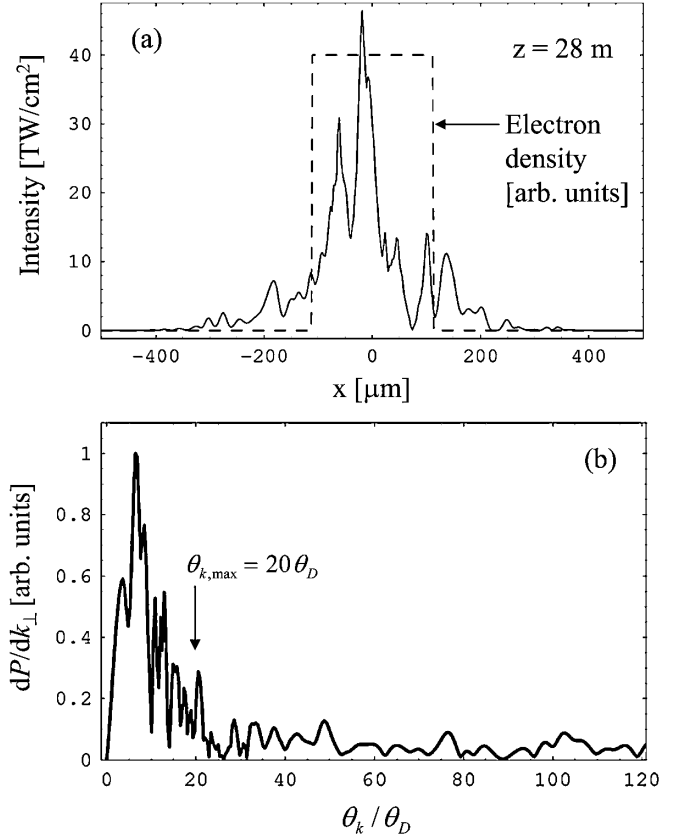


FIG. 8. (a) GENESIS simulation result showing transverse profile of intensity (solid curve) at $z = 28 \text{ m}$ (saturation) for the LCLS FEL. The dashed curve denotes electron beam profile. (b) Distribution of power over normalized transverse wave number (propagation angle), for the intensity profile shown in (a). The propagation angle is normalized to the diffraction angle θ_D and $\theta_{k,\text{max}}$ denotes the maximum propagation gain angle used in calculating the theoretical coherent power in Fig. 7.

plots the power as a function of propagation distance within the wiggler. The blue curve is the result of a GENESIS simulation. The dashed curve and solid black curves represent the theoretically calculated incoherent and coherent power, respectively. The theoretical incoherent and coherent power are functions of the maximum solid angle as indicated by Eqs. (26) and (30). In calculating the theoretical incoherent power, we assume a maximum solid angle of $\Delta\Omega_{\text{incoh}} = \pi/(3\gamma_{z0})^2$. To calculate the coherent power, we use a maximum angle $\theta_{k,\text{max}}$ consistent with the spectrum of transverse wave numbers generated by the simulation [see Fig. 8(b)]. This angle, to a good approximation, is given by $\theta_{k,\text{max}} \approx r_b/L_g$. The red curve in Fig. 7 represents the total theoretical power at a given interaction length. There is excellent agreement between theory and simulation in both the incoherent ($z < 7$ m) and coherent ($z > 7$ m) regimes.

Figure 8(a) plots the radiation intensity profile at saturation and shows that it is highly localized to the region of the electron beam. Figure 8(b) shows the distribution of power over transverse wave number, i.e., dP/dk_{\perp} . Most of the power is contained within the angle $\theta_{k,\text{max}}$, which in this case is ~ 20 times larger than the diffraction angle.

B. Laser-pumped x-ray FEL

The parameters used in the laser-pumped FEL are listed in Table I. For these parameters lethargy effects (electron beam slippage) are negligible. Figure 9 shows the evolu-

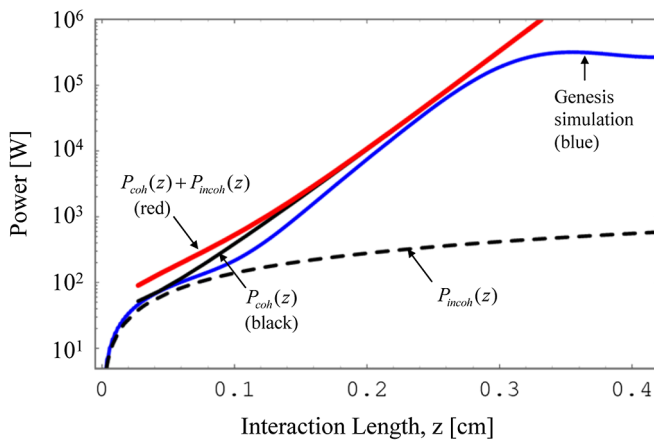


FIG. 9. (Color) Power versus interaction length for a laser-pumped FEL (cold beam) with parameters listed in Table I. Curves denote coherent power (solid black), incoherent power (dashed), total theoretical power (red), and the result of a GENESIS simulation (blue). The theoretical efficiency is $\eta = 0.023(\lambda_o/L_{g0}) = 0.008\%$. The efficiency observed in the GENESIS simulation is 0.01%. In calculating the incoherent and coherent power from Eqs. (26) and (30), we used the maximum angle resolved by the simulation, i.e., $\theta_{\text{sim}} \approx \lambda/(2\Delta_x) = 5 \times 10^{-4}$ rad, where $\Delta_x = 1.6 \mu\text{m}$ is the transverse grid size. In this parameter regime, $\theta_{\text{sim}} \ll \theta_{k,\text{max}}$, where $\theta_{k,\text{max}}$ is the maximum propagation angle of the coherent radiation given by Eq. (16).

tion of the x-ray power as a function of interaction length. The theoretically calculated incoherent and coherent powers are shown separately. In this parameter regime, the transverse resolution of the simulation is not sufficient to resolve the maximum propagation angle. Hence, in calculating the theoretical incoherent and coherent power for comparison with the simulations, the maximum angle is taken to be $\theta_{\text{sim}} = \lambda/(2\Delta_x)$, i.e., the maximum angular resolution of the simulation, where Δ_x is the transverse grid size. The transition from incoherent to coherent radiation occurs after ~ 2 – 3 power gain lengths. The power gain length is $L_{g0} = 280 \mu\text{m}$ while the saturation length is $L_{\text{sat}} \sim 13L_{g0} \sim 0.35$ cm. The conversion efficiency is $\eta = 0.01\%$ which corresponds to a saturated coherent x-ray power of $P_{\text{coh}} = 300$ kW. The theoretical conversion efficiency, in Eq. (13), gives a value of 0.01% in excellent agreement with the GENESIS simulations.

Figure 10(a) plots the transverse x-ray intensity profile at saturation and shows that the radiation is highly localized

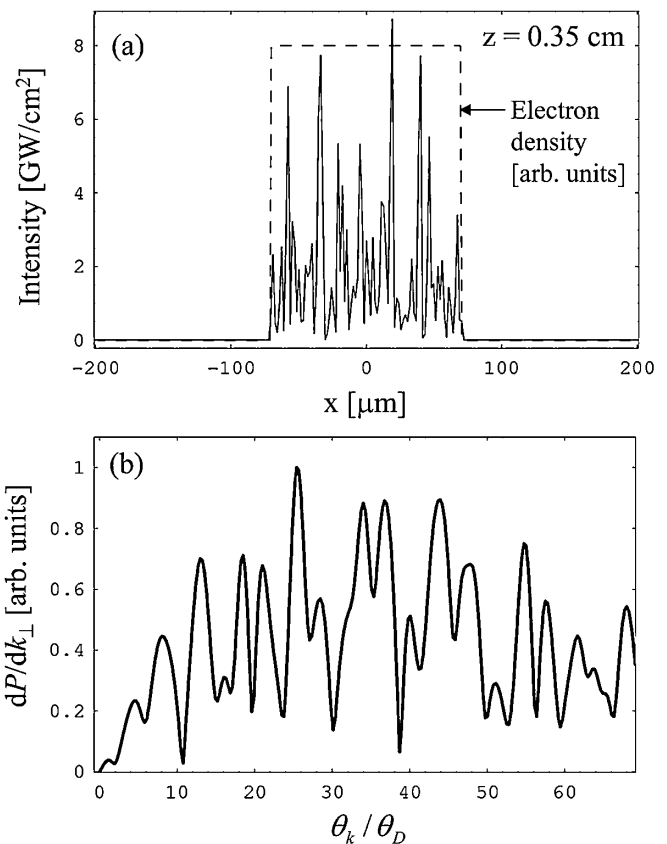


FIG. 10. (a) GENESIS simulation result showing transverse profile of intensity (solid curve) at $z = 0.35$ cm (saturation) for the laser-pumped FEL. The dashed curve denotes electron beam profile. (b) Distribution of power over normalized transverse wave number (propagation angle), for the intensity profile shown in (a). The propagation angle is normalized to the diffraction angle θ_D . The maximum angle resolved by the simulation is $\theta_{k,\text{max}} = 70\theta_D$. The maximum theoretical propagation angle is $\theta_{k,\text{max}} \approx 500\theta_D$.

to the electron beam and contains a large number of higher order transverse modes. Figure 10(b) plots the distribution of power over transverse wave number and shows there is significant power over the entire wave-number range resolved by the simulation.

In this example the required relative electron beam energy spread is $\leq 0.01\%$. Higher electron beam energy spreads would substantially reduce the lasing efficiency and limit the growth of coherent x-ray power. This example indicates the stringent requirements placed on both the electron beam and pump laser.

V. CONCLUSIONS

We have analyzed a high-gain, laser-pumped, x-ray FEL amplifier. The analysis includes (i) electron beam thermal effects, (ii) off-axis propagation, and (iii) the transition from incoherent to coherent x rays. The power gain length, saturation length, linewidth, and conversion efficiency have been calculated for the laser-pumped FEL. We find there is good agreement between our theoretical results and GENESIS simulations. For electron beams of sufficiently high quality, with energies of ~ 6 MeV and currents of 500 A, we find that coherent x rays at 20 Å can be generated with power gain lengths of ~ 300 μm , saturation lengths of ~ 0.4 cm, and conversion efficiencies of 0.01%. To achieve these values the fractional electron beam energy spread must be $< 0.01\%$. The inclusion of higher-order modes in the pump laser can reduce the resonant frequency spread due to transverse gradients to $< 0.01\%$. However, restricting the longitudinal variation of, or the longitudinal variation of pump laser to广播 acceptable levels will be difficult. While a coherent x-ray source would have aagonizingly attractive features, the requirements placed onнде both the electron 2007 and pump laser无可争辩 are challenging.

ACKNOWLEDGMENTS

This work was supported by NRL and ONR.

[1] Linac Coherent Light Source Conceptual Design Report, SLAC Report No. SLAC-R-593, UC-414, 2002.
 [2] TESLA Technical Design Report, TESLA FEL Report No. 2002-09, DESY, 2002.
 [3] SPring-8 Compact SASE Source Conceptual Design Report, <http://www.xfel.spring8.or.jp>, 2005.
 [4] I. S. Ko, in *Proceedings of the 2005 Free Electron Laser Conference* (Stanford University, Stanford, CA, 2005), p. 216.
 [5] T. C. Marshall, *Free-Electron Lasers* (MacMillan, New York, 1985).
 [6] C. A. Brau, *Free-Electron Lasers* (Academic, San Diego, CA, 1990).
 [7] H. P. Freund and T. M. Antonsen, *Principles of Free-Electron Lasers* (Chapman & Hall, London, UK, 1992).

[8] W. B. Colson, Nucl. Instrum. Methods Phys. Res., Sect. A **237**, 1 (1985).
 [9] C. W. Roberson and P. Sprangle, Phys. Fluids B **1**, 3 (1989).
 [10] P. G. O'Shea and H. P. Freund, Science **292**, 1853 (2001).
 [11] P. Sprangle, J. Plasma Phys. **11**, 299 (1974).
 [12] L. R. Elias, W. M. Fairbank, J. M. J. Madey, H. A. Schwettman, and T. I. Smith, Phys. Rev. Lett. **36**, 717 (1976).
 [13] N. M. Kroll and W. A. McMullin, Phys. Rev. A **17**, 300 (1978).
 [1 4] A. A. Kolomenskii 4 (1978).).
 [15] P. Sprangle and A. T. Drobot, J. Appl. Phys. **50**, 2652 (1979).
 [16] P. Sprangle and R. A. Smith, Phys. Rev. A **21, 293 (1980).
 [17]] P. Sprangle, C. M. Tang, and W. M. Manheimer, Phys. Rev. A 21, 302ial
 [18] N. M. Kroll, P. L. Morton, and M. N. Rosenbluth, IEEE J. Quantum Electron. **17**, 1436 (1981 warta
 [19] D. Pro, 24, 1436 (1981).
 [20] R. Bonifacio, C. Pellegrini, and L. Narducci, Opt. Commun. **50**, 373 (1984).
 [21] K. made, Phys. Rev. Lett. <1986).
 [22] C. Pellegrini, Nucl. Instrum. Methods Phys. Res., Sect公共预算. A **445**, 1241 (2000).
 [23] Z. Huang and K. J. Kim, Nucl. Instrum. Methods Phys. Res., Sect. A **507
 [24] Z. Huang and K. J. Kim, Phys.shaw Rev. ST Accel. Beams , 034801 (2007).
 [ted] J. B Spotlight and C. Pellegrini, J. Opt. Soc. Am. B **2**, 259 (1985).
 [26] N. Piovella,ong, Phys. Plasmas **6**, 3358 (1999).
 [27] R. H. Pantell, G. Soncini, and H. E. Puthoff, IEEE J. Quantum Electron. **4**, 905 (1968).
 [28] P. Sprangle and V. L. Granatstein, Appl. Phys. Lett. **25**, 377 (1974).
 [29] J. Gea-Banacloche, G. T. Moore, R. R.才能得到. Schlicher, M. O. Scully, and H. Walther, IEEE J. Quantum Electron. **23**, 1558 (1987).
 [30] P. Sprangle, B. Hafizi, and F. Mako, Appl. Phys. Lett. **55**, 2559 (1989).
ogos, Nucl. Instrum. Methods Phys. Res., Sect. 475, 190 (2001).
 [32] C. Pellegrini, in Proceedings of the 2005 Free Electron Laser Conference (Ref. [4]), p. 203; S. Tantawi, V. Dolgashev, C. Nantista, C. Pellegrini, J. Rosenzweig, and G. Travish, in Proceedings of the 2005 Free Electron Laser Conference (Ref. [4]), p. 438.
 [33] A. Bacci, M. Ferrario, C. Maroli, V. Petrillo, and L. Serafini, Phys. Rev. ST Accel. Beams **9**, 060704 (2006).
 [34] S. Reiche, Nucl. Instrum. Methods Phys. Res., Sect. A **429**, 243 (1999).
 [35] G. T. Moore, Nucl. Instrum. Methods Phys. Res., Sect. A **239**, 19 (1985).
 [36] R. Bonifacio, Nucl. Instrum. Methods Phys. Res., Sect. A **546**, 634 (2005).
 [37] R. Bonifacio, N. Piovella, and G. R. M. Robb, in Proceedings of the 2005 Free Electron Laser Conference****

- (Ref. [4]), p. 664.
- [38] N. Piovella, M.M. Cola, L. Volpe, A. Schiavi, and R. Bonifacio, Phys. Rev. Lett. **100**, 044801 (2008).
- [39] M. Reiser, *Theory and Design of Charged Particle Beams* (Wiley-VCH, Berlin, Germany, 2008).
- [40] E. Esarey, S. K. Ride, and P. Sprangle, Phys. Rev. E **48**, 3003 (1993).
- [41] C. A. Brau, Phys. Rev. ST Accel. Beams **7**, 020701 (2004).
- [42] G. A. Krafft, A. Doyuran, and J. B. Rosenzweig, Phys. Rev. E **72**, 056502 (2005).
- [43] W. M. Fawley, Nucl. Instrum. Methods Phys. Res., Sect. A, **507**, 19 (2003).